Available online at www.sciencedirect.com
ScienceDirect
Trans. Nonferrous Met. Soc. China 32(2022) 1822−1833
Transactions of Nonferrous Metals Society of China
www.tnmsc.cn

Tailoring microstructure and mechanical properties of aluminum matrix composites reinforced with novel Al/CuFe multi-layered core-shell particles

Rashid ALI[1], Fahad ALI[1], Aqib ZAHOOR[1], Rub Nawaz SHAHID[1], Naeem ul Haq TARIQ[1], Zafar IQBAL[1], Adnan Qayyum BUTT[2], Saad ULLAH[1], Hasan Bin AWAIS[1]

1. Department of Metallurgy and Materials Engineering, Pakistan Institute of Engineering and Applied Sciences (PIEAS), Islamabad, Pakistan;
2. Materials Division, Pakistan Institute of Nuclear Science and Technology (PINSTECH), Islamabad, Pakistan

Received 1 July 2021; accepted 16 December 2021

Abstract: Aluminum matrix composites (AMCs), reinforced with novel pre-synthesized Al/CuFe multi-layered core-shell particles, were fabricated by different consolidation techniques to investigate their effect on microstructure and mechanical properties. To synthesize multi-layered Al/CuFe core-shell particles, Cu and Fe layers were deposited on Al powder particles by galvanic replacement and electroless plating method, respectively. The core-shell powder and sintered compacts were characterized by using X-ray diffraction (XRD), scanning electron microscopy (SEM) equipped with energy dispersive spectroscopy (EDX), pycnometer, microhardness and compression tests. The results revealed that a higher extent of interfacial reactions, due to the transformation of the deposited layer into intermetallic phases in spark plasma sintered composite, resulted in high relative density (99.26%), microhardness (165 $HV_{0.3}$) and strength (572 MPa). Further, the presence of un-transformed Cu in the shell structure of hot-pressed composite resulted in the highest fracture strain (20.4%). The obtained results provide stronger implications for tailoring the microstructure of AMCs through selecting appropriate sintering paths to control mechanical properties.

Key words: core-shell reinforcement; aluminum matrix composites; electroless plating; sintering techniques; spark plasma sintering; interfacial reaction

1 Introduction

Current industrial modernization requires multifunctional materials which simultaneously possess more than one excellent property. Generally, structural materials should have good strength and ductility with good thermal stability. Similarly, high-speed trains simultaneously require metallic wires with high electric conductivity as well as good wear resistance. However, some properties rarely co-exist concurrently. For instance, toughness and strength devour each other, viz. increasing strength will impair toughness or vice versa [1,2]. To cater to the curbs of conventional materials, composite materials are developed to meet modern industrial requirements [3,4]. Among these composites, Al matrix composites (AMCs) have a perspective for high-tech applications due to their incredible mechanical properties and corrosion resistance coupled with low density [5−9]. To enhance the properties of Al matrix composites for industrial requirements, micron-sized particulate reinforcements are being developed in-situ during consolidation. The advantages of in-situ methods are the improvement in the high-temperature

Corresponding author: Fahad ALI, E-mail: fahadali62@hotmail.com
DOI: 10.1016/S1003-6326(22)65911-9

performance because of thermodynamically stable reinforcement's formation, and good interfacial bonding at interfaces [10,11]. From these in-situ developed reinforcements, specially tailored micro-structures are synthesized. For instance, core-shell structures are used in the fields of electronics, catalysts, batteries and biomedical materials etc. However, applications of core-shell particles in the field of structural materials are motivating researchers to further explore their potential [12−14]. Recently, the formation of hard and brittle intermetallic shells around a ductile core (Fe, Ni, Ti and Cu) has been reported due to in-situ interfacial reactions during the processing of AMCs [12−14]. In such core-shell particulates reinforced aluminum matrix composites (CS-PRAMCs), crack propagation is restricted or delayed by moderating their tip during plastic deformation of metal (pure Al in the matrix and metallic core), which results in the improvement of ductility [15,16].

In this regard, pre-synthesized core/multi-shell reinforcements can potentially provide better resistance to crack propagation in AMCs as compared to single shell reinforcements. But, AMCs with such reinforcements have not been explored yet. In this respect, Al/CuFe multi-shell reinforcements can be of special interest as Cu−Fe systems have been reported to exhibit excellent characteristics (high wear resistance and strengthening in AMCs due to interfacial reaction) [17,18]. Although the processing of these immiscible elements (Cu−Fe) is difficult due to their positive heat of mixing, their combination can be processed to form egg-like core-shell structures [19]. AMCs, reinforced with quasicrystals (AlCuFe based), show the combination of lower strength and fracture strain as compared to the present AMCs (reinforced with pre-synthesized Al/CuFe core-shell particles) [20]. This further highlights the significance of the multi-layered core-shell reinforcements for AMCs. Additionally, the low density of Al core provided additional benefits in reducing thermal stress and density of the composite [20]. In this study, considering the idea of CS-PRAMCs and extraordinary properties of immiscible elements (Cu−Fe), multi-layered Al/CuFe core-shell particles were prepared by depositing submicron layers of copper and iron on Al particles by replacement and electroless plating methods, respectively. The synthesized particles were subsequently incorporated in the Al matrix as the reinforcement. Materials containing multi-shell microstructures (such as abalone) can exhibit considerably enhanced mechanical characteristics including the combination of strength and toughness. However, such structures have not been extensively explored in AMCs. Moreover, a contiguous network of such structures (Al/Cu and Al_7Cu_2Fe) may enhance thermal/electrical conductivity, strength and wear resistance [3,20]. Such composites can be potentially applied in transport and miniaturized electronic industries. It was anticipated that the deposited layers will transform in-situ into different (binary and ternary) intermetallic phases because of the reaction of Al (in matrix and core) depending on the sintering technique used [21,22]. In the sintering process, green powder compact is subjected to heating to increase contact areas between particles by decreasing porosity, rounding of contact points, and reduction of interconnected pores by grain growth.

Higher sintering temperature, prolonged sintering time, grain growth and low densification in the final products are the vital limitations associated with the conventional vacuum sintering (VS) process. To overcome these limitations, other techniques of hot-pressing (HP) and spark plasma sintering (SPS) have been realized by the researchers. These techniques result in improved densification, microstructure and mechanical properties [23,24]. In HP, pressure and temperature are applied simultaneously in a vacuum or an inert atmosphere. The applied load facilitates breakage of the oxide layer and increases diffusion rate to yield better characteristics in the product. Whereas, SPS process results in better characteristics in composites (high densification, fine microstructure and surface cleaning) as compared to other sintering techniques. The main features of SPS are low sintering temperature, reduced sintering time, high heating rate, and environment-friendly technique, wherein pressure and temperature are simultaneously applied in a controlled environment. To the best of our knowledge, this is the first study exploring the impact of consolidation path on densification, microstructure and mechanical behavior of AMCs reinforced with pre-synthesized multi-layered Al/CuFe core-shell particulates.

2 Experimental

To synthesize Al/CuFe powder, spherical Al powder (purity > 99.5% and particle size D_{50}: 10 μm) was used for deposition of copper and iron. The deposition process comprised three steps: surface pretreatment, Cu deposition and Fe deposition. Initially, 2.0 g of Al particles were pretreated (etched) in 50 mL alkaline solution (5 mL of 33% ammonia solution and 45 mL distilled water) for 2 min. Then, this slurry was poured directly in a preheated (55 °C) copper deposition bath at pH 9.0, adjusted with 33% ammonia solution. After 15 min, Al/Cu core-shell powder particles were filtered and washed with hot water. In the next step, these particles were again immersed in the preheated (80 °C) iron deposition bath for 10 min at pH 9.2. The detailed baths compositions for copper and iron depositions are given follows [25,26]: (1) Copper bath: 0.10 mol/L copper sulfate ($CuSO_4·5H_2O$) as the main salt, 0.20 mol/L ethylene diamine tetraacetic acid disodium (EDTA-2Na·$2H_2O$) as a complexing agent, 0.005 mol/L copper chloride ($CuCl_2$) and 0.5 mol/L boric acid (H_3BO_3) as a buffer [25]; (2) Iron bath: 0.10 mol/L iron sulfate ($FeSO_4·7H_2O$) as the main salt, 0.22 mol/L sodium potassium tartrate ($KNaC_4H_4O_6·4H_2O$) as a complexing agent, 0.03 mol/L citric acid ($C_6H_8O_7$), 0.40 mol/L sodium hypophosphite ($NaH_2PO_2·H_2O$) as reducing agent and 0.5 mol/L boric acid (H_3BO_3) as a buffer [26].

Finally, particles were filtered and washed thrice with hot water and dried for 8 h at 80 °C. The density of Al/CuFe composite powder was measured by a helium gas pycnometer (AccuPyc-II 1340) to calculate the volume fraction (20%) of reinforcement Al/CuFe in the Al matrix. The Al and pre-synthesized Al/CuFe powders were blended with a dry powder rotator (Glas Col, LLC) rotated at 70 r/min for 1 h.

The obtained blend was uniaxially pressed at 640 MPa and room temperature to obtain a cold compacted cylinder with 10 mm in diameter and 10 mm in length. This green compact was sintered by using VS at 520 °C for 240 min. The remaining blended powder was also subjected to HP and SPS for comparison. The blend was hot-pressed at 640 MPa and 520 °C for 20 min in an inert argon atmosphere in the induction heated die. Similarly, SPS was performed in a graphite die (20 mm in diameter and 5 mm in thickness) at 50 MPa and 520 °C for 5 min. The detailed process flow is shown in Fig. 1.

From VS and HP samples (10 mm in diameter and 10 mm in length), three specimens (3 mm in

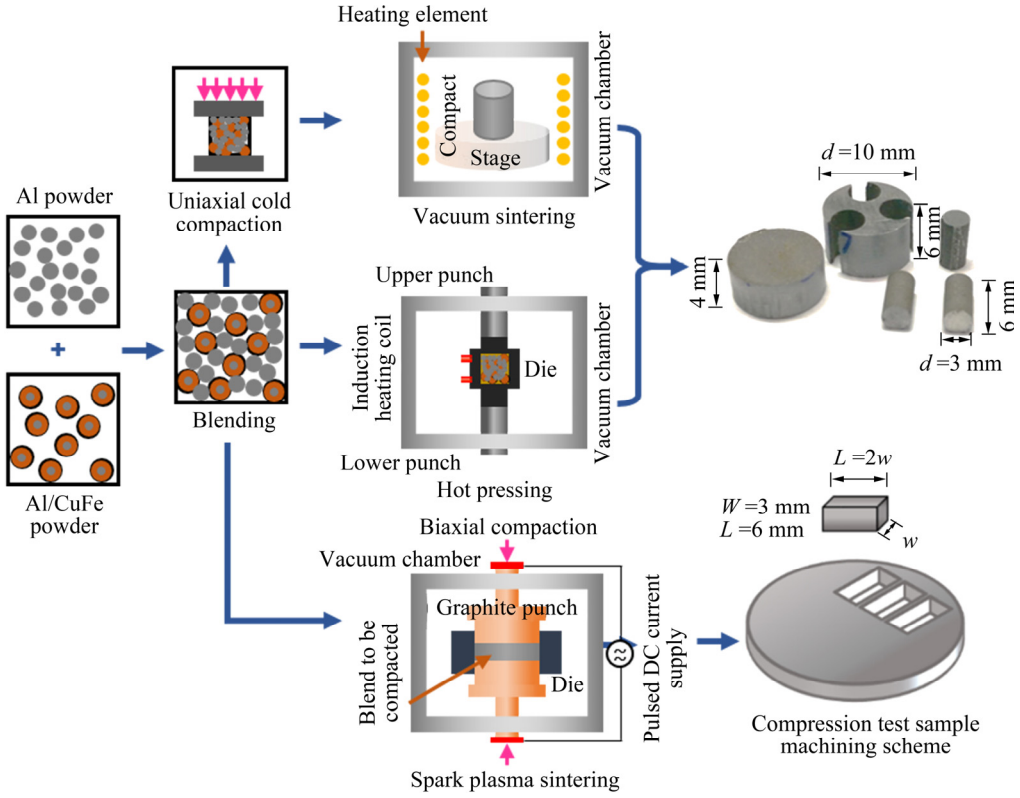

Fig. 1 Process flow for fabrication of composites by VS, HP and SPS

diameter and 6 mm in length) from each composite were machined, by using electrode discharge machining (wire cut), for quasi-static compression tests. Similarly, from SPS compact, three samples (with dimensions of 3 mm × 3 mm × 6 mm) were machined for compression tests. Compression tests were performed at room temperature according to ASTM E9—2009 standard at a constant strain rate of 10^{-4} s^{-1}. Identification of elements and phases in pre-synthesized powder and sintered composites was carried out by X-ray diffraction (Philips PW 1050 Bragg-Brentano diffractometer) with Cu K_α radiation (0.154 nm) source. The influence of sintering techniques on microstructure, the integrity of interfaces and analysis of fractured samples were investigated by Tescan MAIA3 field emission scanning electron microscope (FE-SEM) with an in-built energy dispersive X-ray spectrometer (EDX). The density of composites was measured by using a pycnometer. The Vickers microhardness tester (Tinius Olsen FH 14) at 0.3 kg load for 15 s was used to measure the microhardness of composites to investigate the sintering effect. Eight hardness values were measured for each composite to avoid any uncertainty.

3 Results and discussion

3.1 Characterization of Al/CuFe multi-layered core-shell powder

Figure 2(a) shows the SEM micrograph of as-received Al particles used in this study. The initial smooth surface of Al particles becomes rough after copper deposition. Initially, an adherent, dense and rough layer of submicron copper grains was deposited, covering most of the Al particle surface (Fig. 2(b)). Afterward, the Fe layer was deposited on Al/Cu particles. The EDX line scanning (Fig. 2(c)), surface mappings (Figs. 2(d−f)) of single-particle and its cross-section (Figs. 2(g−j)) confirm the deposition of Cu and Fe layers on Al particles. There are two visible rings of Fe in Fig. 2(j). The first outer ring is due to the direct deposition of iron on the pre-deposited copper layer.

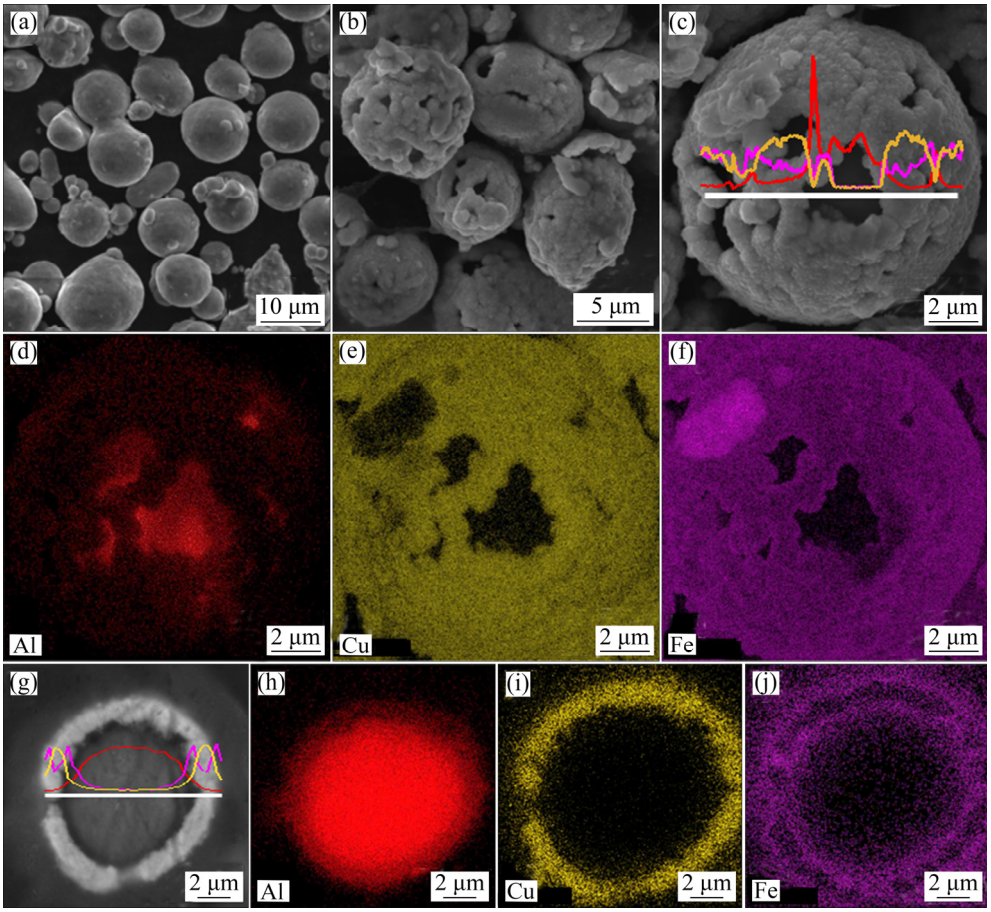

Fig. 2 SEM micrographs of Al (a), Al/CuFe composite powder (b), Al/CuFe particle with EDX line scan (c), surface mappings of single-particle (d−f), cross-sectional view of Al/CuFe powder particle with EDX line scan (g) and surface mappings of cross section (h−j)

While, the inner ring is due to Fe deposition in gaps present in the copper layer, and direct reduction of Fe ions on Al substrate because of partial delamination of Al from Cu shell. From SEM results, it can be deduced that the Cu deposit initially has the cauliflower morphology which transforms to angular grains after Fe deposition. The schematic process diagrams along with the corresponding SEM images (showing particle surface morphology) are shown in Figs. 3(a) and (b). For Fe deposition on a Cu substrate, it is well established that the Al surface is needed to be in contact with Cu [27,28]. Al works as a sacrificial element at this stage which results in delamination or dissolution of Al in particles (Fig. 3(c)). Al dissolution can be minimized by providing extra Al surface by inserting 02 pre-etched Al strips with dimensions of 25 mm × 25 mm in an iron deposition bath. Moreover, as these particles were compacted before or during the sintering process, this Al delamination may not be problematic. The measured density (5.26 g/cm^3) of Al/CuFe core-shell powder was used to calculate the volume fraction (20%) of reinforcement.

Figure 4(a) presents the XRD results of the uncoated Al particles, Cu-coated Al powder (Al/Cu) and Fe-coated Al/Cu powder (Al/CuFe). The diffracted peaks of Al are observed at 2θ values of 38.6°, 44.8°, 65.2°, 78.3°, 82.6°, 99.7°, 111.9°, and 115°. After Cu plating, new peaks are visible at 2θ values of 43.2°, 50.6°, 74.1°, 90.1°, and 95.4°, corresponding to the FCC Cu crystal structure. Similarly, after Fe deposition, the Al/CuFe powder was analyzed by XRD. The characteristic peaks of Fe are superimposed on Al peaks at 2θ values of 44.8°, 65.2°, 82.6°, and 98.9°. The increase in the intensity of Al peaks at 2θ values of 44.8° confirms the iron deposition. Consequently, the visible characteristic peaks in XRD patterns of synthesized composite powders, after the deposition of copper

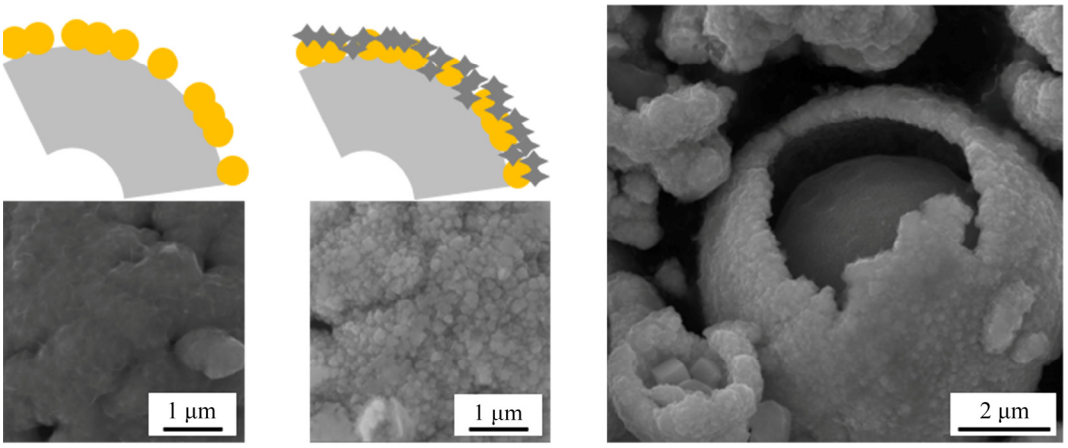

Fig. 3 Schematic deposition process description with high magnification SEM images for surface morphology of particle after copper plating (a), iron plating (b) and delamination of Al particle from deposited layers (c)

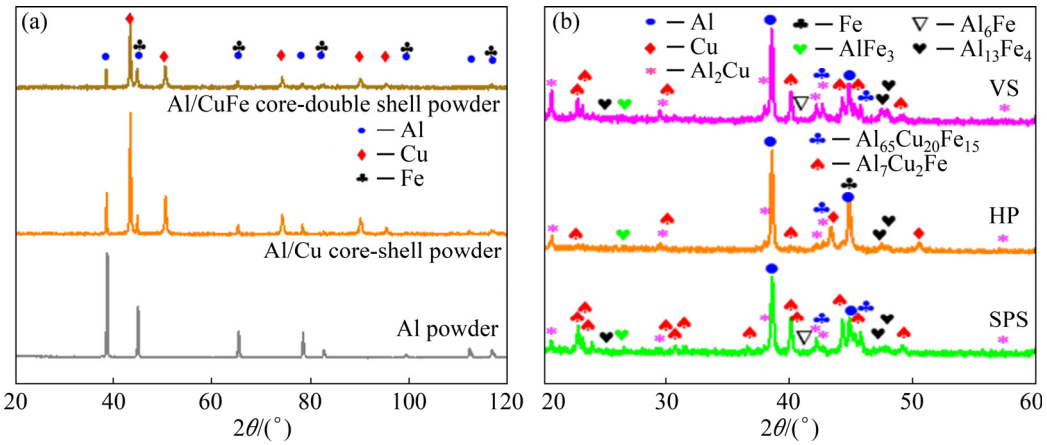

Fig. 4 XRD patterns of Al, Al/Cu and Al/CuFe powders (a), and sintered (VS, HP and SPS) composites (b)

(Al/Cu) and copper−iron (Al/CuFe), correspond to Cu, Fe and Al only (Fig. 4(a)). There is no visible peak other than these basic constituents.

3.2 Effect of sintering technique

3.2.1 XRD patterns of composites

The XRD patterns of AMCs (reinforced with 20 vol.% Al/CuFe duplex powder) sintered by VS, HP, and SPS at 520 °C are shown in Fig. 4(b). From binary phase diagrams, five stable intermetallic phases in each system of Al−Fe ($AlFe_3$, AlFe, Al_2Fe, Al_5Fe_2 and Al_3Fe) and Al−Cu (Al_2Cu, AlCu, Al_4Cu_9, Al_3Cu_4 and Al_2Cu_3) are probable in the solid-state diffusion couple [29−31]. Moreover, Al−Cu−Fe ternary intermetallics (such as $Al_{65}Cu_{20}Fe_{15}$ and Al_7Cu_2Fe) are also possible in the sintered composites [32−34]. These phases may form due to the in-situ transformation of deposited layers into intermetallic phases at the interfaces. During this transformation, aluminide formation due to the larger atomic flux of Al into Cu and Fe is more probable [35]. However, the formation of these expected intermetallic phases depends upon the thermodynamics and kinetics of the sintering process. The XRD patterns show that there are six phases developed in VS, HP and SPS composites (Al_2Cu, $AlFe_3$, Al_7Cu_2Fe, $Al_{65}Cu_{20}Fe_{15}$, $Al_{13}Fe_4$ and Al_6Fe) other than Al, Cu and Fe. However, a comparison of peak intensities in XRD scans illustrates that major phases, formed during all consolidation processes, are Al_7Cu_2Fe and Al_2Cu.

Generally, the oxide layer prevents diffusion across the interfaces between Al and Cu. But, plastic deformation during compaction in HP and SPS results in breakage of the oxide layer. This rupturing of the oxide layer results in enhanced densification in a relatively short time. On the other hand, the complete transformation of Cu and Fe metallic coatings into intermetallic phases is attributed to the prolonged sintering time in VS due to long-range diffusion. Whereas, deposited CuFe layers in HP composite were not completely transformed. This unreacted ductile Cu and Fe may affect the mechanical behavior of the fabricated composites. In SPS, the generation of intense heat at interfaces and surface cleaning effect are responsible for the completion of diffusion reactions between composite constituents. Alike VS, there is no evidence of unreacted Cu or Fe.

3.2.2 Microstructure

The SEM micrographs of all the sintered composites, illustrating the distribution of Al/CuFe particulate reinforcements in the Al matrix, are shown in Fig. 5 along with elemental mappings. The darker area indicates Al in the matrix as well as in the inner core while brighter areas express CuFe shells or Cu/Fe aluminides. The contrast variation validates the changes in the elemental concentration profile due to the interfacial reactions of Al (in matrix and core) and deposited (CuFe) shells during sintering. During the consolidation of composites, the deposited Cu and Fe in reinforcing particles transform into intermetallic phases due to the interfacial reactions. In these interfacial reactions, aluminides are formed which have a considerably higher volume than Cu and Fe. Moreover, the consolidation path decides the extent of transformation (XRD Fig. 4(b)). The higher degree of transformation results in a higher fraction of intermetallic area in SEM micrographs. In HP, the pressure and temperature were applied simultaneously for a relatively short time, which results in the densification of the composite due to the presence of unreacted soft Cu and Fe (Fig. 5(b)), which is evident from XRD results. Moreover, the shape and thickness of CuFe shells do not change in the hot-pressed sample (Figs. 5(a) and (d)) as compared to other studied samples. At higher magnification, the SEM micrograph (yellow arrows in Fig. 5(d)) shows that all interfaces are well bonded in the hot-pressed composite. The interfaces between Al and CuFe shell and between CuFe−CuFe shells in agglomerated reinforcement particles are soundly joined together. The iron and copper distribution in EDX mappings (Figs. 5(g−i)) of hot-pressed composite indicates that the multi-shell structure of Cu and Fe layers remains intact.

In contrast, the prolonged VS process results in extensive diffusional interfacial reactions, which is evident from the thicker layer of intermetallic phases around reinforcing particles. Furthermore, the core-shell feature of the composite microstructure is extensively distorted due to the prolonged diffusional processes in VS sample. Moreover, it was reported that Cu diffuses more deeply in Al as compared to Al in Cu [35]. As a result, small grains of Al_2Cu can be formed in the matrix (Figs. 5(b) and (e)) away from reinforcing

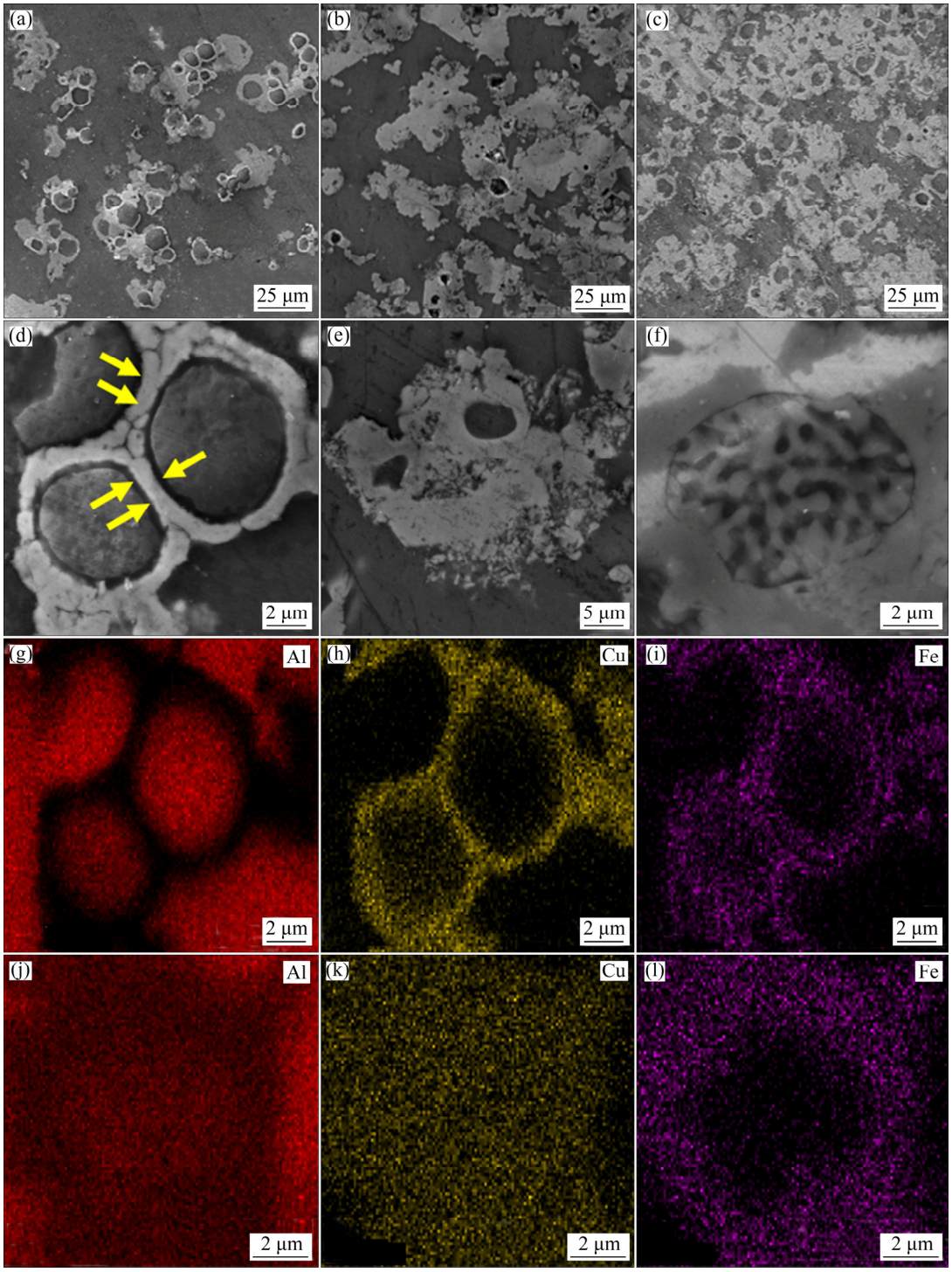

Fig. 5 SEM micrographs of composites prepared by HP (a, d), VS (b, e) and SPS (c, f) and elemental mappings of composites prepared by HP (g−i) and SPS (j−l)

particles. The third composite sample was consolidated using the SPS process (Fig. 5(c)). This process is known to have the following features: oxide-free rapid densification, intense heating and low grain coarsening. The intense heating results in the complete conversion of CuFe multi-shell into intermetallic phases. Moreover, intense heating in SPS results in the formation of localized lamellar structure within the core of reinforcing particles (Fig. 5(f)). The elemental mappings (Figs. 5(j−l)) of this area show that Fe has not diffused in the core area and lamellae consist of eutectic of Al and Al_2Cu phases. Nevertheless, the interfacial layer is thinner as compared to that of VS composite.

Additionally, in contrast to VS, most of the reinforcing particles retain their initial spherical shape after the consolidation.

3.2.3 Physical and mechanical properties

Figure 6(a) reveals the influence of sintering mode on the densification of the composites. For computing relative density, initial density was foreseen by the rule of mixture. The density results show that, despite a longer sintering period in VS process, the composite sample shows lower relative density (97.46%) in comparison to HP and SPS samples. This means that a higher fraction of porosity is present in VS sample. The presence of a higher fraction of porosity can be attributed to: (1) limitation of the vacuum sintering process due to the absence of external pressure, (2) formation of porosity due to difference in diffusion coefficients of composite constituents (larger difference in diffusion coefficients of Al in Cu or Fe than Cu or Fe in Al at the current experimental temperature of 520 °C causes Kirkendall's effect, and the Kirkendall's effect promotes porosity formation at interfaces [36]), and (3) molar volumetric changes due to extensive in-situ transformation reactions, which are evident from the absence of Cu peaks in the XRD pattern shown in Fig. 4(b). During HP, a higher relative density of 99.8% is achieved due to the simultaneous application of external pressure and temperature. The oxide layer on Al and reinforcing particles provide a diffusion barrier, which lowers the sintering ability of the composite. The applied force breaks down the oxide layer during hot pressing and results in lower porosity or higher relative density than those of vacuum sintering. Usually, in SPS, the DC pulse discharge develops heating, spark plasma and spark impact pressure. The spark discharge in the openings between particles causes a localized rise of the temperature (up to 10^4 °C). Such extraordinary temperature results in momentary vaporization and melting of surfaces of particulates. Moreover, the surface cleaning in the SPS process increases the diffusion rate which results in better densification of the compact. Therefore, SPS is an effective method to acquire a fully dense composite. In this study, the composite sample consolidated by the SPS route shows 99.2% of relative density. However, it is worth mentioning that there is a slight decline in densification in the SPS sample as compared to that in the HP sample. This slight reduction in density can be related to the volumetric changes associated with a higher fraction of intermetallic phases during SPS as compared to the HP sample. This is quite evident in the XRD pattern shown in Fig. 4(b). The XRD scan shows the presence of the unreacted ductile Cu and Fe in the HP sample, which further facilitates the densification in the HP composite sample.

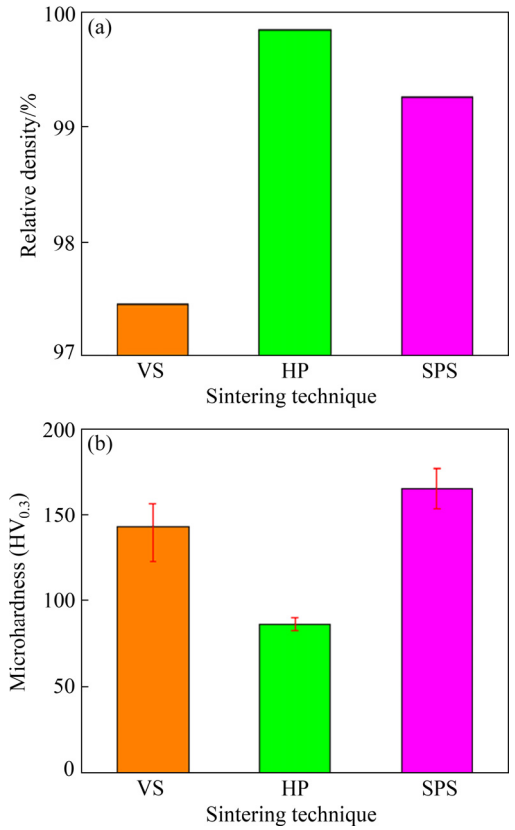

Fig. 6 Effect of sintering technique (VS, HP and SPS) on relative density (densification) (a) and microhardness (b) of composites

The influence of sintering techniques (VS, HP and SPS) on the mechanical performance of the prepared composites was evaluated by conducting microhardness and uniaxial compression tests. The effect of the sintering route on Vickers microhardness is presented in Fig. 6(b). The results indicate that microhardness increases in order: HP (85 $HV_{0.3}$) < VS (143 $HV_{0.3}$) < SPS (165 $HV_{0.3}$). From these hardness values, it can be concluded that a higher degree of interfacial reactions leads to the improved microhardness. In VS composites, the prolonged sintering time results in complete transformation of deposited Cu and Fe shells into hard intermetallic phases (Fig. 4(b)). The prolonged sintering time also results in grain coarsening

(Fig. 5(b)). Overall, the microhardness of VS samples lies between that of HP and SPS samples. Despite the high volume fraction of intermetallic phases, its hardness is lower than that of SPS samples due to grain coarsening and lower density. The lowest hardness of HP composite is due to the incomplete interfacial transformation of soft and ductile Cu and Fe layers into aluminides despite its highest density. In the SPS process, the shortest sintering time at a higher heating rate results in reduced grain coarsening. The localized intense heating at particle interfaces results in the complete transformation of deposited Cu and Fe shells into intermetallic phases. Thus, the highest hardness is observed in SPS composites. Moreover, concurrent application of pressure and temperature in SPS enhances the density of the product, which results in the improved hardness.

The compression test results of different composites are summarized in Figs. 7(a) and (b). The results elucidate that the sintering technique has a prominent impact on the compressive behavior of the prepared AMCs. It should be noticed that pure Al compacts, consolidated by such techniques, have a maximum compressive strength (UCS) of 155 MPa [37,38]. In the present work, the compressive strength increases from 155 MPa for pure Al to 389, 403 and 572 MPa for the composites consolidated by VS, HP and SPS routes, respectively. Transformation of deposited layers into intermetallic, due to prolonged diffusion, results in wide interfacial reaction zones in VS. Accordingly, VS composites exhibit higher hardness and yield strength (YS) than reported pure Al compacts. Similarly, SPS composites display the highest compressive strength due to the complete transformation of deposited layers into intermetallic phases. Consequently, a higher volume fraction of hard intermetallic phases and reduced matrix ligament size (due to the intermetallic phase distribution) result in considerably large improved mechanical strength. Whereas, relatively moderate strength, along with the highest toughness as compared to other investigated consolidation techniques, is observed in HP composite.

From compression test results, it can be concluded that the extent of interfacial reaction between composite constituents (Al, Cu and Fe) has a substantial influence on the toughness of fabricated composites. The unconsumed Cu in HP

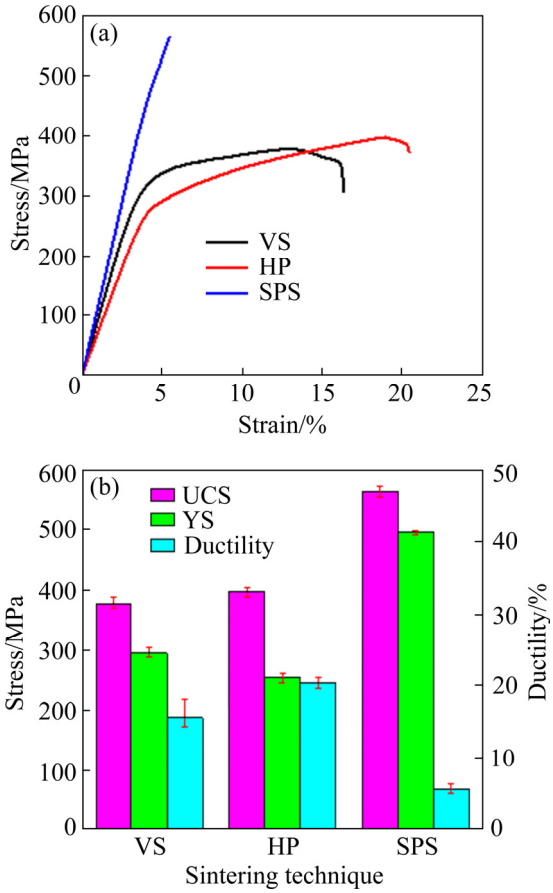

Fig. 7 Effect of sintering technique (VS, HP and SPS) on compressive stress−strain curves (a) and summary of results (b)

composite (Fig. 4(b)) results in toughening of composites. It is expected that cracks, initiated in intermetallic layers, would be arrested in the soft Al (in matrix and core) and un-reacted Cu and Fe shells. This crack arresting phenomenon results in delaying the crack propagation, thus the highest ductility (20.4%) in HP composites is experienced.

The reduced ductility observed in VS (15.6%) and SPS (5.5%) can be attributed to two reasons: (1) thicker layer of intermetallic phases has greater susceptibility to catastrophic crack propagation, and (2) higher extent of interfacial reactions is responsible for the creation of porosities at interfaces. From this study, it can be established that the mechanical properties of the Al matrix reinforced with Al/CuFe core-shell morphology can be tailored by carefully controlling the fabrication parameters.

After the compression test, the fractured samples of all composites were scanned by SEM (Fig. 8) to examine the effect of the sintering route

on fracture behavior. The shear bands are visible in all composites. These bands present ductile fracture of the Al matrix (grey color contrast). As discussed previously, the complete transformation of the deposited shells (CuFe) into brittle intermetallic phases (white color contrast) was observed in VS and SPS composites (Fig. 4(b)). These hard intermetallic phases are responsible for the reduced fracture strain of these composites as compared to HP samples. Additionally, the fraction of intermetallic phases (formed during consolidation) was estimated by analyzing SEM images using ImageJ software. Results showed that intermetallic area fraction (A_f) increases in the order: ${}^{HP}A_f < {}^{VS}A_f < {}^{SPS}A_f$. Hence, brittle facets can be seen in the fracture micrographs of VS and SPS composites as shown in Fig. 8(a, c). This corroborates well with the least fracture strain and presence of brittle facets in the SPS sample. Moreover, the phenomenon of crack arresting in the soft-Al core is evident in Fig. 8(d), which was the main objective of using core-shell reinforcement. In contrast, the smaller grains of intermetallic phases (estimated from FWHM of Al_2Cu and Al_7Cu_2Fe intermetallic phases) are developed in-situ in the CuFe shell during the SPS due to intense heating for a shorter time (Fig. 8(f)). The smaller granular structure of intermetallic shells in the SPS sample as compared to that of VS composite (yellow arrows Fig. 8(f)) improves the strength with a significant decrease in toughness. In HP composite, a higher fraction of unconsumed Cu and Fe results in a ductile shear fracture like Al matrix (Figs. 8(b) and (e)). Moreover, due to the shearing, the sphericity of the reinforcing particulates is slightly distorted under compressive loading.

4 Conclusions

(1) The pre-synthesized Al/CuFe particulate reinforcement (in Al matrix composites) was in-situ transformed into intermetallic phases (major phases: Al_2Cu and Al_7Cu_2Fe) during consolidation.

(2) The prolonged sintering time in VS process and intense heating at interfaces in the SPS process result in the complete transformation of the deposited phases (Cu and Fe layers of core-shell particulates) into intermetallic phases. While, in HP composite, basic constituents of reinforcements do not transform completely.

(3) The relative density, microhardness and compressive strength of the synthesized composites mainly depend upon the degree of interfacial reactions during the consolidation process. With increasing volume fraction of intermetallic phases, relative density decreases while microhardness and compressive strength increase in order from HP to VS to SPS.

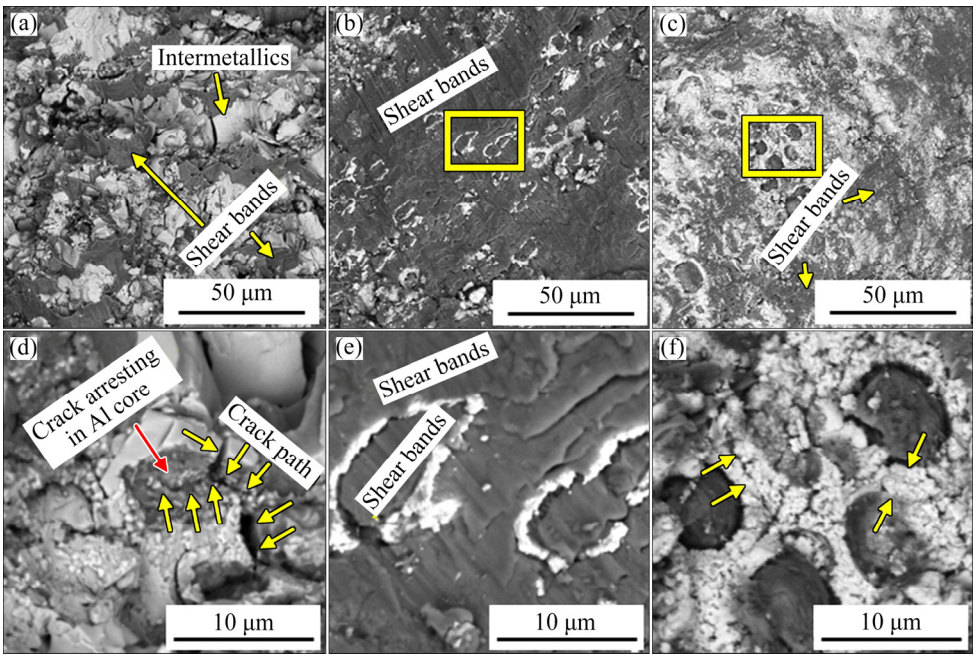

Fig. 8 SEM micrographs representing morphology of fractured surfaces of VS (a, d), HP (b, e), and SPS (c, f) composites

(4) The unconsumed ductile Cu and Fe in particulate reinforcement shells help to improve fracture strain by enhancing crack arresting characteristics. Accordingly, the observed ductility decreases from 20.4% for HP to 15.6% for VS and 5.5 % for SPS.

(5) The findings of this study provide useful implications for the development of AMCs to meet current industrial requirements.

References

[1] WU Xiao-lei, YANG Mu-xin, YUAN Fu-ping, WU Gui-lin, WEI Yu-jie, HUANG Xiao-xu, ZHU Yun-tian. Heterogeneous lamella structure unites ultrafine-grain strength with coarse-grain ductility [J]. Applied Physical Science, 2015, 112: 14501−14505.

[2] ZHANG Y S, ZHAO Y H, ZHANG W, LU J W, HU J J, HUO W T, ZHANG P X. Core-shell structured titanium−nitrogen alloys with high strength, high thermal stability and good plasticity [J]. Science Report, 2017, 7: 40039.

[3] ZHANG Y Y, HEIM F M, BARTLETT J L, SONG N N, ISHEIM D, LI X D. Bioinspired, graphene-enabled Ni composites with high strength and toughness [J]. Science Advances, 2019, 5: 1−10.

[4] CHEN Ti-jun, GAO Min, TONG Yun-qi. Effects of alloying elements on the formation of core-shell-structured reinforcing particles during heating of Al−Ti powder compacts [J]. Materials, 2018, 11: 138.

[5] HAN Tie-long, WANG Fu-cheng, LI Jia-jun, ZHAO Nai-qin, HE Chun-nian. Simultaneously enhanced strength and ductility of Al matrix composites through the introduction of intragranular nano-sized graphene nanoplates [J]. Composites (Part B): Engineering, 2021, 212: 108700.

[6] GUAN H D, LI C J, GAO P, YI J H, BAO R, TAO J M, FANG D, FENG Z X. Fe-based metallic glass particles reinforced Al-7075 matrix composites prepared by spark plasma sintering [J]. Advanced Powder Technology, 2020, 31: 3500−3506.

[7] JARGALSAIKHAN B, BOR A, LEE J Y, CHOI H K. Al/CNT nanocomposite fabrication on the different property of raw material using a planetary ball mill [J]. Advanced Powder Technology, 2020, 31: 1957−1962.

[8] NTURANABO F, MASU L, KIRABIRA J B. Novel applications of aluminium metal matrix composites [C]//Aluminium Alloys and Composites. London: Intech Open, 2019: 13.

[9] JOSEPH A, GAUTHIER-BRUNET V, JOULAIN A, BONNEVILLE J, DUBOIS S, MONCHOUX J P, PAILLOUX F. Mechanical properties of Al/ω-Al−Cu−Fe composites synthesized by the SPS technique [J]. Materials Characterization, 2018, 145: 644−652.

[10] YANG Hong-yu, DONG Er-ting, ZHANG Bing-qi, YUAN Yan-yan, SHU Shi-li. Fabrication and characterization of in situ synthesized SiC/Al composites by combustion synthesis and hot press consolidation method [J]. Scanning, 2017, 2017: 1−11.

[11] AZARNIYA A, AZARNIYA A, ABDOLLAH-ZADEH A, MADAAH HOSSEINI H R, RAMAKRISHNA S. In situ hybrid aluminum matrix composites: A review of phase transformations and mechanical aspects [J]. Advanced Engineering Materials, 2019, 21: 1801269.

[12] CHEN Ti-jun, GENG Li-bo, QIN He, GAO Min. Core-shell-structured particle reinforced A356 matrix composite prepared by powder-thixoforming: Effect of reheating temperature [J]. Materials, 2018, 11: 1−20.

[13] XUE Yang, SHEN Ru-juan, NI Song, SONG Min, XIAO Dai-hong. Fabrication, microstructure and mechanical properties of Al−Fe intermetallic particle reinforced Al-based composites [J]. Journal of Alloys and Compounds, 2015, 618: 537−544.

[14] LIU Yi-xiong, ZHENG Zhen-xing, CAO Geng-hua, ZHU De-zhi, YANG Chao, LUO Ming-qiang. Interface structure and mechanical properties of 7075Al hybrid composite reinforced with micron Ti metal particles using pressure infiltration [J]. Metals, 2019, 9: 763.

[15] YADAV D, BAURI R. Development of Cu particles and Cu core-shell particles reinforced Al composite [J]. Materials Science and Technology, 2015, 31: 494−500.

[16] WU Wen-qian, GUO Bai-song, XUE Yang, SHEN Ru-juan, NI Song, SONG Min. Ni−Al_xNi_y core-shell structured particle reinforced Al-based composites fabricated by in-situ powder metallurgy technique [J]. Materials Chemistry and Physics, 2015, 160: 352−358.

[17] MOSKALEWICZ T, KOT M, WENDLER B. Microstructure development and properties of the AlCuFe quasicrystalline coating on near-α titanium alloy [J]. Applied Surface Science, 2011, 258: 848−859.

[18] ALI F, SCUDINO S, ANWAR M S, SHAHID R N, SRIVASTAVA V C, UHLENWINKEL V, STOICA M, VAUGHAN G, ECKERT J. Al-based metal matrix composites reinforced with Al−Cu−Fe quasicrystalline particles: Strengthening by interfacial reaction [J]. Journal of Alloys and Compounds, 2014, 607: 274−279.

[19] WANG C P, LIU X J, OHNUMA I, KAINUMA R, ISHIDA K. Formation of immiscible alloy powders with egg-type microstructure [J]. Science, 2002, 297: 990−993.

[20] LITYŃSKA-DOBRZYŃSKA L, DUTKIEWICZ J, STAN-GŁOWIŃSKA K, WAJDA W, DEMBINSKI L, LANGLADE C, CODDET C. Characterization of aluminium matrix composites reinforced by Al−Cu−Fe quasicrystalline particles [J]. Journal of Alloys and Compounds, 2015, 643: s114−s118.

[21] MA Si-ming, ZHANG Xue-zheng, CHEN Ti-jun, WANG Xiao-ming. Microstructure-based numerical simulation of the mechanical properties and fracture of a Ti−Al_3Ti core-shell structured particulate reinforced A356 composite [J]. Materials and Design, 2020, 191: 108685.

[22] GUO Bai-song, SONG Min, ZHANG Xin-ming, CEN Xi, LI Wei, CHEN Biao, WANG Qi-wei. Achieving high combination of strength and ductility of Al matrix composite via in-situ formed Ti−Al_3Ti core-shell particle [J]. Materials Characterization, 2020, 170: 110666.

[23] GUAN H D, LI C J, GAO P, PRASHANTH K G, TAN J, ECKERT J, TAO J M, YI J H. Aluminum matrix composites reinforced with metallic glass particles with core-shell structure [J]. Materials Science and Engineering A, 2020, 771:

138630.
[24] IBN-MOHAMMED T, RANDALL C A, MUSTAPHA K B, GUO J, WALKER J, BERBANO S, KOH S C L, WANG D, SINCLAIR D C, REANEY I M. Decarbonising ceramic manufacturing: A techno-economic analysis of energy efficient sintering technologies in the functional materials sector [J]. Journal of the European Ceramic Society, 2019, 39: 5213−5235.
[25] ALI R, ALI F, ZAHOOR A, SHAHID R N, TARIQ N U H, ULLAH S, AHMED R, AWAIS H B. A Taguchi approach to synthesise Al/Fe core-shell composite powders through electroless deposition [J]. Transactions of the IMF, 2021, 99: 265−273.
[26] ALI R, ALI F, ZAHOOR A, NAWAZ SHAHID R, UL HAQTARIQ N, ULLAH S, MAHMOOD A, SHAH A, BIN AWAIS H. Synthesis of Al/Cu core-shell particles through optimization of galvanic replacement method in alkaline solution [J]. International Journal of Materials Research, 2021, 112: 439−447.
[27] HUANG G F, HUANG W Q, WANG L L, MENG Y, XIE Z, ZOU B S. Electrochemical study of electroless deposition of Fe−P alloys [J]. Electrochimica Acta, 2006, 51: 4471−4476.
[28] RUSCIOR C, CROIAL E. Chemical iron−phosphorus films [J]. Journal of the Electrochemical Society, 1971, 118: 696.
[29] GUO Ya-jie, LIU Gui-wu, JIN Hai-yun, SHI Zhong-qi, QIAO Guan-jun. Intermetallic phase formation in diffusion- bonded Cu/Al laminates [J]. Journal of Materials Science, 2011, 46: 2467−2473.
[30] NOVÁK P, MICHALCOVÁ A, MAREK I, MUDROVÁ M, SAKSL K, BEDNARČÍK J, ZIKMUND P, VOJTĚCH D. On the formation of intermetallics in Fe−Al system—An in situ XRD study [J]. Intermetallics, 2013, 32: 127−136.
[31] GUEYDAN A, DOMENGÈS B, HUG E. Study of the intermetallic growth in copper-clad aluminum wires after thermal aging [J]. Intermetallics, 2014, 50: 34−42.
[32] PARSAMEHR H, YANG C L, LIU W T, CHEN S W, CHANG S Y, CHEN L J, TSAI A P, LAI C H. Direct observation of growth and stability of Al−Cu−Fe quasicrystal thin films [J]. Acta Materialia, 2019, 174: 1−8.
[33] PARSAMEHR H, LU Y J, LIN T Y, TSAI A P, LAI C H. In-situ observation of local atomic structure of Al−Cu−Fe quasicrystal formation [J]. Scientific Reports, 2019, 9: 1−9.
[34] YIN Shi-long, BIAN Qing, QIAN Li-ying, ZHANG Ai-mei. Formation of $Al_{70}Cu_{20}Fe_{10}$ icosahedral quasicrystal by mechanically alloyed method [J]. Materials Science and Engineering A, 2007, 465: 95−99.
[35] LI Chang, LI Dong-xu, TAO Xiao-ma, CHEN Hong-mei, OUYANG Yi-fang. Molecular dynamics simulation of diffusion bonding of Al−Cu interface [J]. Modelling and Simulation in Materials Science and Engineering, 2014, 22: 065013.
[36] HE Yue-hui, JIANG Yao, XU Nan-ping, ZOU Jin, HUANG Bai-yun, LIU C T, LIAW P K. Fabrication of Ti−Al micro/nanometer-sized porous alloys through the Kirkendall effect [J]. Advanced Materials, 2007, 19: 2102−2106.
[37] SHAHID R N, SCUDINO S. Microstructural strengthening by phase transformation in Al−Fe_3Al composites [J]. Journal of Alloys and Compounds, 2017, 705: 590−597.
[38] ZENG Wen, YU Da-liang, MA Yi-long, QIU Ri-sheng, CAO Xian-long, DENG Hong-da, LI Chun-hong, SHAO Bin, GUO Dong-lin, LAN Wei. Microstructure and mechanical properties of Al−TiCN composites prepared by spark plasma sintering [J]. Materials Research Express, 2019, 6: 126514.

新型 Al/CuFe 多层核壳颗粒增强铝基复合材料的显微组织和力学性能

Rashid ALI[1], Fahad ALI[1], Aqib ZAHOOR[1], Rub Nawaz SHAHID[1],
Naeem ul Haq TARIQ[1], Zafar IQBAL[1], Adnan Qayyum BUTT[2], Saad ULLAH[1], Hasan Bin AWAIS[1]

1. Department of Metallurgy and Materials Engineering,
Pakistan Institute of Engineering and Applied Sciences (PIEAS), Islamabad, Pakistan;
2. Materials Division, Pakistan Institute of Nuclear Science and Technology (PINSTECH), Islamabad, Pakistan

摘　要：采用不同烧结工艺制备新型 Al/CuFe 多层核壳颗粒增强铝基复合材料(AMCs)，研究其对显微组织和力学性能的影响。分别采用电置换法和化学镀法在铝粉颗粒上沉积 Cu 层和 Fe 层，制备多层 Al/CuFe 核壳颗粒。采用 X 射线衍射(XRD)、扫描电子显微镜(SEM)/能谱(EDX)、密度计、显微硬度和压缩试验等方法对复合材料进行表征。结果表明，在放电等离子烧结复合材料中，由于沉积层向金属间化合物相转变，界面反应程度提高，复合材料的相对密度(99.26%)、显微硬度(165 $HV_{0.3}$)和强度(572 MPa)均显著提高。此外，热压复合材料壳层结构中存在的未转化 Cu 导致其断裂应变最高(20.4%)。研究结果对通过选择合适的烧结路径来调整 AMCs 的显微组织和控制其力学性能具有重要意义。

关键词：核壳增强相；铝基复合材料；化学镀；烧结工艺；放电等离子烧结；界面反应

(Edited by Wei-ping CHEN)